The Variability of Translocator Protein Signal in Brain and Blood of Genotyped Healthy Humans Using In Vivo ^{123}I-CLINDE SPECT Imaging: A Test–Retest Study

Ling Feng*[1], Per Jensen*[1,2], Gerda Thomsen[1], Agnete Dyssegaard[1], Claus Svarer[1], Lars V. Knudsen[1], Kirsten Møller[3], Carsten Thomsen[4], Jens D. Mikkelsen[1,2], Denis Guilloteau[5], Gitte M. Knudsen[1,2], and Lars H. Pinborg[1,2,6]

[1]Neurobiology Research Unit, Rigshospitalet, Copenhagen, Denmark; [2]Faculty of Health and Medicine, University of Copenhagen, Copenhagen, Denmark; [3]Department of Neuroanaesthesiology, Rigshospitalet, Copenhagen, Denmark; [4]Department of Radiology, Rigshospitalet, Copenhagen, Denmark; [5]UFR de Médecine, Université François Rabelais de Tours, France; and [6]Epilepsy Clinic, Department of Neurology, Rigshospitalet, Copenhagen, Denmark

^{123}I-CLINDE is a radiotracer developed for SPECT and targets the 18-kDa translocator protein (TSPO). TSPO is upregulated in glial cells and used as a measure of neuroinflammation in a variety of central nervous system diseases. The aim of this study was to examine the test–retest variability of ^{123}I-CLINDE binding in healthy subjects. **Methods:** SPECT scans were acquired over 90 min in 16 healthy controls (9 women, 8 mixed-affinity binders [MABs] and 8 high-affinity binders [HABs] twice with an interval of 35 ± 15 d). Arterial input functions were based on individual blood measurements in 8 subjects and a population-based approach in combination with individual whole-blood time–activity curves in the other 8 subjects. Seven brain volumes of interest were extracted and quantified by SUVs and by 2-tissue-compartment modeling for calculation of distribution volumes (V_T). Test–retest variability was measured by percentage difference (PD), the absolute PD, intraclass correlation coefficient (ICC), and coefficient of variation. **Results:** The absolute PD of brain SUV and the V_T had similar values. The ICC values were higher for V_Ts than for brain SUVs, which were both moderate to high; however, lower ICC values were observed when calculated separately for HABs and MABs. Test–retest reproducibility was higher in subjects with immediate centrifugation of blood samples. The population-based method efficiently recovered data with delayed centrifugation. The V_T of a 49-y-old male HAB was 7.5 ± 1.4 mL/cm^3 compared with 4.6 ± 1.4 mL/cm^3 of a sex- and age-matched MAB. The SUVs of a 49-y-old male HAB and MAB were 1.03 ± 0.14 and 0.88 ± 0.15 g/mL, respectively. **Conclusion:** The test–retest reproducibility of ^{123}I-CLINDE is comparable or better than that reported for commonly used PET TSPO tracers. Because of the binding of ^{123}I-CLINDE to blood cells and peripheral tissues, SUV is not a sufficient surrogate of V_T from 2-tissue-compartment modeling. The population-adjusted method has the potential to reduce the complexity of blood analyses of TSPO tracers.

Key Words: TSPO imaging; variability; polymorphism; second-generation TSPO tracer

J Nucl Med 2017; 58:989–995
DOI: 10.2967/jnumed.116.183202

In brain parenchyma, the translocator protein (TSPO) is predominantly expressed by glial cells (astrocytes and microglia). Subcellularly, TSPO is mainly located in the outer mitochondrial membrane and functioning as a transporter of cholesterol and porphyrins and importer of proteins (*1*). In the blood, TSPO is expressed mainly in monocytes and polymorphnuclear neutrofils and to a lesser extent in other white blood cells, platelets, and erythrocytes (*2*).

After brain injury, TSPO levels are increased within activated microglia and astrocytes, inspiring the investigation of TSPO as a biomarker of brain injury and repair in brain diseases such as stroke, glioma, and neurodegenerative disorders (*3–6*). TSPO molecular imaging is currently exclusively performed in research protocols but may have future clinical roles in diagnosis and therapeutic drug monitoring in neuroinflammatory disorders.

Test–retest variability is a way to assess the usefulness of radioligands; a radioligand with high reproducibility is better suited for longitudinal studies and requires smaller sample sizes in group comparisons. So far, TSPO imaging test–retest studies have demonstrated moderate to good reproducibility for ^{11}C-PK11195 (*7*) and better reproducibility for the second-generation tracers ^{11}C-DPA-713 (*8*) and ^{11}C-PBR28 (*9,10*).

^{123}I-CLINDE is a SPECT TSPO ligand (*11*). ^{123}I-CLINDE SPECT imaging has previously been applied in patients with stroke, glioblastoma multiforme, and anti *N*-methyl-D-aspartate receptor encephalitis (*12–14*). ^{123}I-CLINDE is susceptible to the rs6971 polymorphism, which affects the affinity of the radioligand binding to the TSPO and separates individuals into high-affinity binders (HABs), mixed-affinity binders (MABs), and low-affinity binders (*15*).

The aim of the current study was to examine the test–retest reproducibility measured as percentage difference (PD) and reliability measured as intraclass correlation coefficient (ICC) and coefficient of variation (COV) of ^{123}I-CLINDE binding in healthy subjects based on the brain SUV and 2-tissue-compartment modeling (2TCM) with arterial blood as the input function.

MATERIALS AND METHODS

Subjects and Genotyping

This study was conducted in accordance with the Declaration of Helsinki at the Copenhagen University Hospital, Rigshospitalet, Denmark. The ethical committee of the Copenhagen Capital Region

Received Aug. 27, 2016; revision accepted Oct. 21, 2016.
For correspondence or reprints contact: Ling Feng, Neurobiology Research Unit, Rigshospitalet, Copenhagen, Denmark.
E-mail: ling.feng@nru.dk
*Contributed equally to this work.
Published online Nov. 10, 2016.

(H-2-2010-086) approved the study protocol. All subjects provided written informed consent.

Because of low TSPO signal in glioblastoma tissue from a patient who was a low-affinity binder (*12*), we did not expect to obtain reliable TSPO signals in healthy low-affinity binders. Consequently, after screening for the rs6971 polymorphism (*12*), 16 healthy subjects (MAB-to-HAB, 1:1; 9 women) were included and SPECT-scanned twice with an interval of 35 ± 15 d. All healthy subjects had normal physical and neurologic examinations and blood tests. Table 1 shows a summary of age, sex, TSPO genotype, and scan information.

Arterial Blood Sampling and Centrifugation

From a radial arterial cannula, blood samples for measuring radioactivity in plasma and whole blood were drawn manually at 0.25, 0.5, 0.75, 1, 1.5, 2, 2.5, 3, 4, 6, 8, 10, 12, 15, 20, 25, 30, 35, 45, 65, and 85 min after injection of ^{123}I-CLINDE. Additionally, samples were drawn at 0.5, 4, 10, 20, 30, 45, 65, and 85 min for metabolite analysis by radio–high-performance liquid chromatography (HPLC) (*16*). Fractions of HPLC eluent were collected using a fraction collector device (Foxy Jr FC144; Teledyne Isco) and counted off-line in a well-counter (2480 Wizard2 γ-Counter; Perkin Elmer) for accurate measurements of parent tracer. For the first 8 subjects, the blood was stored on ice for an estimated 30–90 min until centrifugation (Eppendorf centrifuge 5800R with 3,500 rpm at 4°C in 7 min). During the course of the study, we discovered that ^{123}I-CLINDE continued to bind to TSPO in formed blood cells, presumably the monocytes, until separating plasma from the sample by centrifugation. For the remaining 8 subjects, all blood samples were stored on ice and centrifuged within a maximum of 5 min. The total radioactivity in plasma and whole blood was measured in a well-counter (Cobra 5003; Packard Instruments), and data were decay-corrected to the time of injection. Further, the radioligand purity was measured for each batch of ^{123}I-CLINDE, and trapping efficiency of the HPLC column (plasma control) was determined for each scan by spiking water and blank plasma with ^{123}I-CLINDE. All equipment was cross-calibrated to the SPECT scanner. Blood screening including white blood cell differential count was performed at each scan.

Image Acquisition

To block thyroidal uptake of free radioiodine, 200 mg of potassium perchlorate were administered intravenously 20 min before injection of ^{123}I-CLINDE. A headband was applied to minimize head movements during scanning. Dynamic SPECT scanning with a triple-head IRIX camera (Philips Medical) was started simultaneously with a bolus injection of ^{123}I-CLINDE (MAP Medical Technologies) and lasted for 90 min. The protocol consisted of 10 × 2 min frames, followed by 7 × 10 min frames.

T1-weighted MRI was acquired once for each subject using a 3-T Prisma MR scanner (Siemens) 3 ± 49 d (mean ± SD; median, 0 d) after the corresponding SPECT scan. All brain scans were normal as interpreted by a neuroradiologist.

Image Analysis

Image Preprocessing. For each subject, the weighted mean SPECT image was coregistered to the T1-weighted MR image by interactive image overlay (*17*). Automatic delineation of volumes of interest (VOIs) was performed using probability maps and a data processing pipeline (*18*). Because of the limited spatial resolution of SPECT images, no segmentation of gray matter, white matter, and cerebrospinal fluid was attempted. Seven VOIs were investigated in this study: midbrain, thalamus, pons, striatum, hippocampus, cerebellum (without vermis), and neocortex. These VOIs were defined as volume-weighted means of either the left- and the right-hemisphere or of smaller VOIs: striatum as the mean of caudate nucleus and putamen and neocortex as the mean of frontal cortex, superior temporal gyrus, medial inferior temporal gyrus, parietal cortex, sensory motor cortex, and occipital cortex.

Brain and Blood Uptake. The radioactive concentrations in blood and brain were studied independently to investigate the test and retest variability. Therefore, PD of the SUV_{mean} was calculated, where SUV (g/mL) was defined as time–activity curve (kBq/mL) in the blood or brain VOIs normalized by the injected dose per body weight (in MBq/kg) (*19*), and SUV_{mean} was defined as the area under the SUV curve normalized by time length.

Kinetic Modeling. A 2TCM with arterial plasma function as input (K_1 to k_4 with a fixed blood volume in brain tissue of 5%) was used to quantify ^{123}I-CLINDE binding as distribution volume (V_T), as this has previously been demonstrated to be the optimal method (*12*).

The arterial input function was generated in 2 ways, depending on the blood sample centrifugation.

Method 1: For Studies with Immediate Centrifugation of Blood Samples. To account for tracer purity and trapping efficiency, the measured parent fraction (PF) from the fraction collector was first fitted by a multiexponential function and adjusted as below:

$$\begin{aligned} PF(\mathrm{t}) &= a_1 \times e^{-b_1 t} + a_2 \times e^{-b_2 t} + a_3 \\ PF\_adj(\mathrm{t}) &= (PF(\mathrm{t}) + \text{purity} - \text{plasma control})/\text{purity} \end{aligned} \quad \text{Eq. 1}$$

The difference between ^{123}I-CLINDE purity and plasma control indicates the part failed to be trapped by the extraction column of the radio-HPLC.

Then the metabolite-corrected plasma input function was calculated as the product of the plasma time–activity curve $Cp(\mathrm{t})$ and the adjusted parent fraction $PF\_adj(\mathrm{t})$:

$$C_{mcp}(\mathrm{t}) = C_p(\mathrm{t}) \times PF\_adj(\mathrm{t}) \quad \text{Eq. 2}$$

Method 2: For Studies with Delayed Centrifugation of Blood Samples. The plasma–to–whole-blood ratio (PoB) and adjusted parent fraction as a function of time were generated for all scans that were accompanied by blood samples undergoing immediate centrifugation. The mean of these functions, respectively, were generated as population-based PoB (*PB_PoB*) and population-based parent fraction (*PB_PF*):

$$\begin{aligned} PoB_i(\mathrm{t}) &= a_i \times \left(1 - e^{-b_i t}\right) + c_i \\ PB\_PoB(\mathrm{t}) &= \sum_{i=1}^{N} PoB_i(\mathrm{t})/N \\ PB\_PF(t) &= \sum_{i=1}^{N} PF\_adj_i(\mathrm{t})/N, \end{aligned} \quad \text{Eq. 3}$$

where N is the number of scans. To generate the metabolite-corrected plasma input function (C_{mcp}), these 2 functions were then applied on the measured whole-blood time–activity curve (C_w) of the studies with delayed centrifugation as below:

$$C_{mcp}(\mathrm{t}) = C_w(\mathrm{t}) \times PB\_PoB(\mathrm{t}) \times PB\_PF(\mathrm{t}) \quad \text{Eq. 4}$$

Image and data preprocessing were performed using MATLAB 8.1 (R2013a; Mathworks Inc.), and kinetic modeling was done using PMOD (version 3.0; PMOD Technologies Inc.).

Statistical Analysis

To evaluate the test–retest reproducibility and variability of ^{123}I-CLINDE, the following 4 matrices were used: PD, absolute PD, ICC, and COV.

PD. Test–retest reproducibility was calculated as the difference between test and retest outcome measures divided by their average, outcome measures being SUV_{mean} of blood or brain uptake, and V_T. The absolute PD was also calculated for comparison to other studies.

ICC. ICC evaluates the reliability by measuring within-subject variability relative to between-subject variability as below:

TABLE 1
Demographic Data and Methodologic Information Specified by Subject

Subject no.	Sex	Age (y)	Body weight (kg)	TSPO genotype	Injected activity (MBq)	Scan interval (d)	Centrifugation	Purity (%)	Plasma control (%)
1	M	61	80	MAB	120.9	21	Delayed	96.1	95.4
					117.8			93.5	91.4
2	M	70	92	MAB	112.2	42	Delayed	95.4	95.4
					123.6			94.9	93.8
3	M	59	76.5	HAB	118.1	35	Delayed	96.4	94.7
					112.0			94.9	93.2
4	F	38	110	HAB	116.3	28	Delayed	96.0	95.0
					114.3			90.7	88.4
5	F	62	70	HAB	119.0	42	Delayed	96.1	95.1
					119.4			96.6	94.0
6	F	58	50	MAB	116.0	28	Delayed	96.1	96.2
					119.7			95.3	91.4
7	F	68	87	HAB	124.8	56	Delayed	92.3	90.1
					115.1			95.2	90.5
8	M	52	94	HAB	118.5	56	Delayed	98.1	93.8
					124.1			89.8	88.5
9	M	42	80	MAB	118.8	28	Immediate	95.7	94.6
					115.8			93.4	90.3
10	F	45	86.2	MAB	117.4	56	Immediate	95.4	94.6
					114.1			94.9	94.7
11	M	35	100	HAB	119.9	56	Immediate	93.0	93.2
					114.4			90.7	89.9
12	F	40	73	MAB	112.0	7	Immediate	92.8	91.8
					130.7			94.7	94.1
13	M	24	95.6	MAB	115.4	14	Immediate	94.4	92.2
					116.0			92.0	90.2
14	F	69	83	MAB	123.0	28	Immediate	94.5	92.7
					127.1			94.4	90.4
15	F	30	68	HAB	105.8	42	Immediate	91.0	82.9
					116.0			91.1	88.1
16	F	34	74.2	HAB	118.4	28	Immediate	Not available	Not available
					116.3			Not available	Not available
Mean ± SD		49 ± 15	82.5 ± 14.4		117.9 ± 4.9	35 ± 15		93.4 ± 1.7	91.4 ± 3.2

$$\mathrm{ICC} = \frac{MSS_{btw} - MSS_{within}}{MSS_{btw} + (k-1)\,MSS_{within}}, \qquad \text{Eq. 5}$$

where

$$MSS_{btw} = \frac{1}{N-1}\sum_{i=1}^{N}\left(\overline{V}_{Ti} - \overline{V}_{T}\right)^2 \quad MSS_{within} = \frac{1}{N}\sum_{i=1}^{N}\sum_{j=1}^{k}\left(V_{Tij} - \overline{V}_{Ti}\right)^2 \qquad \text{Eq. 6}$$

MSS_{btw} is the mean sum of squares between subjects and MSS_{within} is the mean sum of squares within subjects, $\overline{V}_{Ti}$ is the mean of test and retest measures of subject i, and $\overline{V}_{T}$ is the mean of all observations (test and retest of all subjects). V_{Tij} is one of the measures of subject i. N is the number of subjects, and k is the number of repeated measures ($k = 2$). If $MSS_{btw} = 0$ there is no reliability, and ICC $= -1$; if $MSS_{within} = 0$ there is maximum reliability, and ICC $= 1$.

COV. The COV of outcome measures was calculated as the SD divided by the mean across all observations for each VOI.

To test effects of centrifugation, genotype, or the test–retest, a linear model fitting using generalized least squares (GLS) was performed in R (version 3.2.2). In general, a GLS model performs similar to a standard linear model but can furthermore account for a complex covariance structure between observations. In our case, the GLS model allows for different variances between residuals in repeated measures and for correlation between them, unless otherwise stated.

Details about each model applied will be given in the "Results" section. For GLS models, mean and SE are given. In other cases, mean

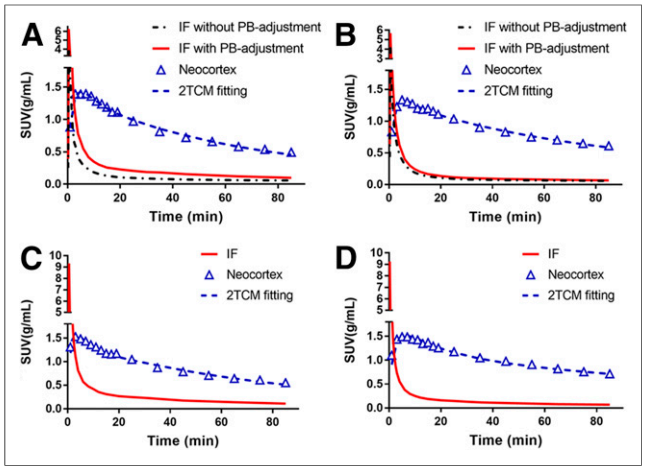

FIGURE 1. The effect of population-based (PB) approach to adjust input functions (IF) with delayed centrifugation (A and B) and SUVs of IF and brain region of MABs (A and C) and HABs (B and D). (A and B) SUVs of MAB (subject 6) and HAB (subject 3), separately, both with delayed centrifugation of blood samples. 2TCM fitting to neocortex using the input functions (red curves) was also given. (C and D) SUVs of MAB (subject 10) and HAB (subject 14), both with immediate centrifugation of blood samples.

and SD are given. The paired-sample *t* test, Wilcoxon rank-sum test, and Pearson linear correlation were performed using MATLAB 8.1 (R2013a; Mathworks Inc.).

RESULTS

The injected radioactivity in test and retest scans was not statistically different, and neither was ^{123}I-CLINDE purity or plasma control (Table 1).

Delayed Centrifugation and Discrepancy Between Blood and Brain PD

In the first 8 subjects with delayed centrifugation of blood samples, we found a large test–retest PD of SUV_{mean} in the plasma parent compound (1.0% ± 31.3%), but much lower PD in the brain (0.7% ± 8.0% - 2.2% ± 18.8% in 7 VOIs).

Effect of Genotype

In subjects with immediately centrifuged samples, the parent fraction SUV_{mean} was higher in MABs (0.37 ± 0.07, mean ± SE) than in HABs (0.22 ± 0.05, mean ± SE; $P = 0.0006$, GLS model, age and sex adjusted), with a MAB-to-HAB ratio of 1.65. A genotype-related difference was also observed in PoB (Supplemental Fig. 1; supplemental materials are available at http://jnm.snmjournals.org). The mean PoB time–activity curve of HABs ($n = 2 \times 3$) and that of MABs ($n = 2 \times 5$) had different kinetics, especially during the first 20 min; however, the difference was not significant. The $SUV_{mean\ 0–20\ min}$ of MABs correlated negatively with monocyte counts ($P = 0.0341$, $R^2 = 0.4486$). A negative trend was also observed for HABs ($P = 0.1938$).

Arterial Input Function

Immediately Centrifuged Blood Samples. After parent fraction adjustment using Equation 1, the parent fraction between MAB and HAB was still significantly different ($P = 0.0002$, GLS model, age and sex adjusted). Furthermore, the parent fraction curves had different starting points: 94% intact ^{123}I-CLINDE left for MABs and 77% for HABs; at 20 min after injection, 53% for MABs and 36% for HABs; and at 90 min, 38% left for MABs and 27% for HABs.

The arterial input function of a MAB and a HAB (Figs. 1C and 1D) showed faster washout in the HAB. Because of the observed differences between genotypes, population-based PoB functions and population-based PF functions were generated separately for these 2 genetic groups. Before applying the population-based functions to adjust data with delayed centrifugation, method validation was done on the data with immediate centrifugation using a leave-one-out procedure, where population-based functions were generated excluding the scan that the functions were applied on.

These *PB_PoB* functions were applied to the whole-blood time–activity curve *Cw* first to estimate the plasma time–activity curve *Cp*. The differences between estimated *Cp* and the measured data were 0.2% ± 4.3% for MABs ($n = 2 \times 5$) and 0.6% ± 10.8% for HABs ($n = 2 \times 3$); none of the differences was significant. Thereafter, *PB_PF* was applied to *Cp* to estimate the metabolite-corrected plasma input function *Cmcp*. Differences between population-adjusted estimates and measured *Cmcp* were 0.6% ± 9.1% for MABs and 0.5% ± 8.0% for HABs; none of the differences was significant.

Delayed Centrifuged Blood Samples. Immediate centrifugation increased the SUV_{mean} of PoB from 0.95 to 1.07 ($P = 0.0003$, GLS model, genotype adjusted), which was 12.4% more than the SUV_{mean} of PoB from subjects whose samples underwent delayed centrifugation (descriptive data of PoB are given in Fig. 2). Thus, the arterial input functions were underestimated in scans with delayed centrifugation of blood samples (Figs. 1A and 1B). Therefore, population-adjusted input functions were calculated in these cases.

After adjustment using *PB_PoB* and *PB_PF* on *Cw*, test–retest PD of *Cp* decreased from −22.7% ± 27.6% to −9.4% ± 15.2% (absolute PD of *Cp* decreased from 27.7% to 14.4%), and PD of *Cmcp* changed from −2.5% ± 34.6% to −6.4% ± 15.5% (absolute PD of *Cmcp* decreased from 28.0% to 14.1%) (Supplemental Fig. 2).

Test–Retest Variability

Brain Uptake. The brain SUV_{mean} of 7 VOIs was studied. The SUV_{mean} of a male HAB and a male MAB, at age 49 y, were 1.03 ± 0.14 and 0.88 ± 0.15 g/mL (mean ± SE), respectively, and

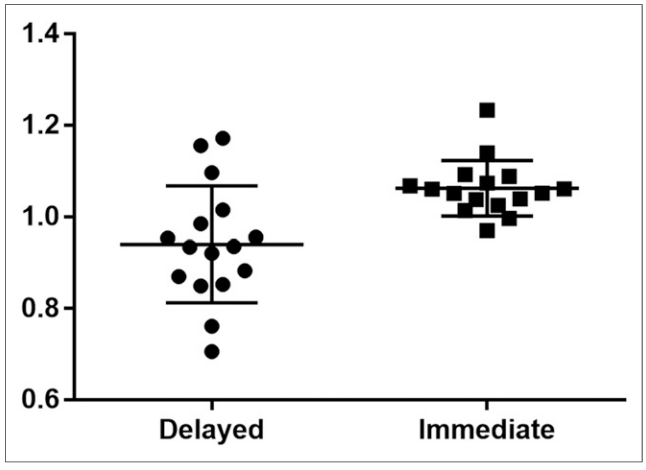

FIGURE 2. Effect of immediate centrifugation of blood samples on PoB.

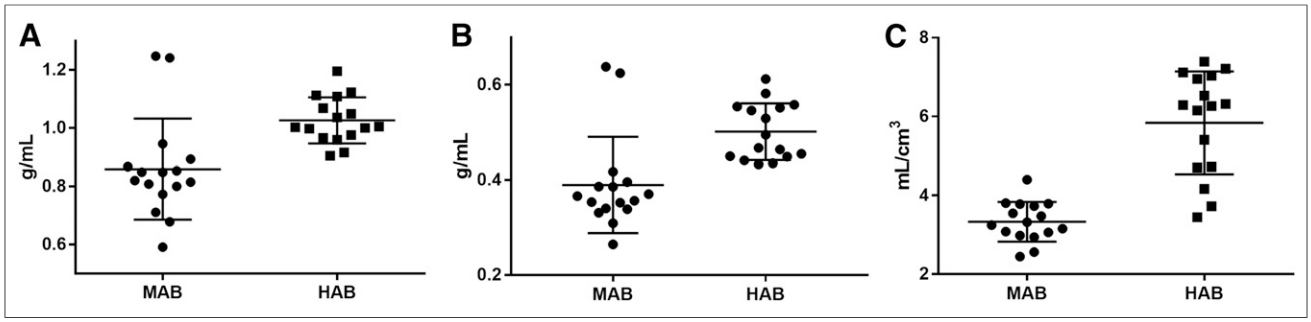

FIGURE 3. Cerebellar brain SUV_{mean} (A), $SUV_{mean\ 60–90\ min}$ (B), and V_T (C) categorized by genotype: MAB and HAB.

the difference was borderline significant ($P = 0.0535$, GLS with different residual variances). The higher binding in HABs than in MABs was also shown in Figure 1, illustrated as SUVs of neocortex with slower washout in HABs. The SUV_{mean} of HABs was 16.8% higher than that of MABs (descriptive data are shown in Fig. 3A). Ten of 16 subjects had lower brain SUV_{mean} in test than retest scans.

Because the beginning of a brain time–activity curve can be influenced by blood flow, $SUV_{mean\ 60–90\ min}$ was also studied. The $SUV_{mean\ 60–90\ min}$ of a male HAB and a male MAB aged 49 y were 0.55 ± 0.09 and 0.43 ± 0.09 g/mL (mean ± SE), respectively ($P = 0.0105$, GLS with different residual variances), and the $SUV_{mean\ 60–90\ min}$ of HABs was 27.6% higher than MABs (descriptive data are provided in Fig. 3B).

The PDs of brain SUV_{mean} across all subjects in 7 VOIs are shown in (Table 2). Test and retest SUV_{mean} of the same subject correlated to a high degree, with correlation coefficients of 0.86 ± 0.07 ($P < 0.05$, $n = 16$). The PD of MABs was on average −3.6% ± 8.1% whereas that of HABs was −7.0% ± 7.8%; however, the difference was not significant (GLS model, age and sex adjusted), and the absolute PD was not sensitive to genotype. ICC values for MABs and HABs and the total samples are given in Table 2. The COV was 20.0% ± 2.3% in MABs and 9.2% ± 2.0% in HABs. Furthermore, ICC and COV differed between MABs and HABs ($P = 2.29e\text{-}05$, $P = 1.38e\text{-}05$, respectively), with a MAB-to-HAB ratio of 1.8 for ICC and 2.2 for COV.

V_Ts. The V_Ts of 7 VOIs derived from 2TCM of scans with immediately and delayed centrifuged blood samples, with and without population-based adjustment of the input functions, are given in Supplemental Tables 1–3. Figure 1 illustrates the 2TCM fitting using the measured or population-based adjusted input functions.

The V_Ts of scans with delayed centrifuged blood samples (16 scans, 7 VOIs) before and after population-based adjustment was significantly different ($P = 0.0176$, GLS with different residual variances), with a V_T value of 5.3 ± 1.1 mL/cm^3 before the adjustment and 4.7 ± 1.1 mL/cm^3 (mean ± SE) after the adjustment. Delayed centrifugation of samples led to an underestimation of input functions and therefore caused an overestimation of the V_Ts by 12.4% on average.

The V_Ts (32 scans, 7 VOIs) of a male HAB and a male MAB aged 49 y (mean age) were 7.5 ± 1.4 and 4.6 ± 1.4 mL/cm^3 (mean ± SE), respectively ($P = 0.0001$, GLS with different residual variances) using population-based adjusted input functions in scans with delayed blood centrifugation and measured input functions in scans with immediate blood centrifugation. V_Ts of HABs were on average 65% higher than MABs, and there was no test–retest difference (Fig. 3C). Test–retest variability measures were calculated for the immediately centrifuged scans and the population-adjusted delayed centrifuged scans both separately and combined (Table 2). For subject 16, the measured purity and plasma standard were not available, thus no adjustment was done.

For the immediately centrifuged scans, test V_T was 0.28 mL/cm^3 lower than retest V_T across all 7 VOIs ($P = 0.0122$, GLS model, age and sex adjusted). This GLS model assumes a homogeneous test–retest difference across VOIs, because

TABLE 2
Test–Retest Variability

	V_T of DC* ($n = 8$)			V_T of IC† ($n = 8$)			V_T of all subjects ($n = 16$)					Brain uptake ($n = 16$)				
Region	PD (%)	Absolute PD (%)	ICC	PD (%)	Absolute PD (%)	ICC	PD (%)	Absolute PD (%)	ICC of MABs	ICC of HABs	ICC of all	PD (%)	Absolute PD (%)	ICC of MABs	ICC of HABs	ICC of all
Midbrain	2.8 ± 14.5	12.4	0.96	−1.5 ± 15.6	11.8	0.86	0.6 ± 14.8	12.1	0.41	0.91	0.93	−2.5 ± 11.5	10.1	0.72	0.39	0.71
Thalamus	11.0 ± 10.5	12.8	0.94	−12.3 ± 13.3	12.7	0.86	−0.7 ± 16.7	12.8	0.68	0.84	0.90	−4.7 ± 14.6	11.6	0.74	0.53	0.71
Pons	−2.3 ± 14.2	9.6	0.90	−8.2 ± 23.8	18.9	0.72	−5.3 ± 19.2	14.2	0.54	0.60	0.82	−2.7 ± 12.4	11.0	0.81	0.52	0.77
Pallidostriatum	5.8 ± 21.9	17.6	0.85	−7.0 ± 19.0	14.1	0.87	−0.6 ± 20.9	15.8	0.22	0.79	0.85	−2.2 ± 13.7	11.1	0.79	0.50	0.74
Hippocampus	14.9 ± 17.3	15.7	0.75	−5.9 ± 11.8	9.7	0.91	4.5 ± 17.9	12.7	0.58	0.78	0.83	−2.0 ± 15.2	12.3	0.57	0.23	0.56
Cerebellum	9.6 ± 9.4	10.2	0.94	−4.9 ± 10.0	8.2	0.96	2.3 ± 12.0	9.2	0.76	0.88	0.95	−1.5 ± 9.4	7.8	0.90	0.45	0.87
Neocortex	5.8 ± 12.6	10.2	0.92	−3.2 ± 12.8	10.5	0.92	1.3 ± 13.2	10.4	0.88	0.79	0.92	−2.8 ± 9.6	8.5	0.91	0.57	0.85

*V_T using population-adjusted input function of delayed centrifugation.
†V_T of immediate centrifugation.

there were no interactions between the 7 VOIs and test–retest scans.

The PD between test–retest of all subjects ($n = 16$) across all 7 VOIs evaluated as repeated measures was on average $-11.7\% \pm 8.6\%$ for MABs and $-12.1\% \pm 8.3\%$ for HABs, and the difference was not significant (GLS, age and sex adjusted). The COV was $16.7\% \pm 3.4\%$ for MABs and $26.5\% \pm 7.7\%$ for HABs. Opposite to the brain SUV_{mean}, ICC and COV estimated by the V_Ts were borderline significantly higher for HABs than MABs ($P = 0.0533$, $P = 0.0492$, respectively), with a HAB-to-MAB ratio of 1.6 for ICC and 1.7 for COV.

DISCUSSION

In this study, we investigated the test–retest variability of the second-generation TSPO SPECT ligand ^{123}I-CLINDE in a group of 16 healthy volunteers.

Population-Based Approach

We used a population-based approach to adjust data from subjects with delayed blood centrifugation. The feasibility of the approach was validated on the immediately centrifuged data in a leave-one-out manner to avoid bias. After adjustment, the test–retest difference decreased in blood components. If time-dependent binding to blood cells is also observed in other TSPO ligands, this approach could be applied to data if centrifugation is delayed. Furthermore, this approach has the potential to reduce the complexity and time consumption associated with blood handling and determination of metabolites, because only whole-blood counts are needed.

^{123}I-CLINDE SPECT Variability

ICC values of V_Ts were higher for ^{123}I-CLINDE SPECT than previously reported in healthy controls for the first-generation TSPO tracer ^{11}C-PK11195 PET (*7*) and comparable to second-generation TSPO tracers such as ^{11}C-PBR28 (*9*) and ^{11}C-DPA-713 (*8*). ICC is a statistical analysis to compare the between-subject variation with the within-subject variation. If HAB and MAB subjects are pooled and not measured separately for each genetic group, ICC values will be higher and reflect not only the variability of the method but also a known biologic difference in affinity. In contrast to previous studies in second-generation TSPO tracers, we also calculated ICC and COV separately for each genetic group, revealing higher ICC and COV values for HABs than MABs. A plausible explanation for a generally modest reliability when subdividing into genotypes is that the TSPO signal, because of its nonprominent presence under healthy conditions, has a relatively low signal-to-background ratio compared with a disease situation with an amplified TSPO signal driven by disease-related activated glial cells. For MABs, the signal-to-background ratio is lower than for HABs, consequently leading to a comparably lower reliability. PD of brain SUV_{mean} and V_T and the absolute PD for ^{123}I-CLINDE SPECT were slightly smaller than previously reported for ^{11}C-PBR28 (*9*).

SUV as Semiquantitative Measure

In a clinical setting, SUV is often used as a semiquantitative surrogate measure to V_T. This is due to several complications related to the complexity of the blood sampling and analysis. In this paper, we studied the genotype difference and test–retest variability using both SUV and V_T to investigate the feasibility of using SUV as an outcome measure for a TSPO ligand. From the brain

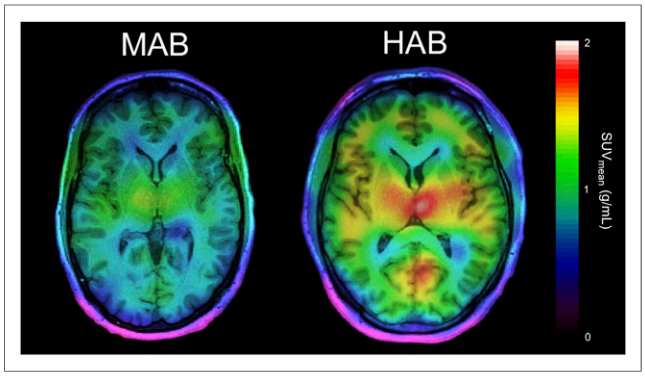

FIGURE 4. Brain SUV_{mean} of typical MAB (subject 12) and HAB (subject 11).

SUV_{mean}, it is possible to differentiate MAB and HAB (Fig. 4), with HABs having an approximately 17% higher binding than MABs when quantified using SUV_{mean} of the whole time–activity curve and approximately 28% higher when quantified using $SUV_{mean\ 60–90\ min}$. However, HABs had on average a 65% higher binding than MABs using V_T estimated by 2TCM modeling. This can be explained by higher affinity of radioligand to TSPO in HABs and the binding of radiotracer to the abundant TSPO in both blood and peripheral tissues. Thus, less free radioligand would be available in the plasma of HABs compared with MABs, which would remain undetected using brain SUV as an outcome. In a clinical setting, patients can have a longitudinally varying disease-related peripheral immune response and thereby varying peripheral TSPO binding sites. This may cause changing concentrations of parent TSPO tracer in the plasma, which as a consequence influences the brain uptake. In Yoder et al. (*20*), SUV was compared with V_T in quantifying TSPO changes in baboons' brain caused by lipopolysaccharide using ^{11}C-PBR28, and SUV failed to detect neuroinflammation as indicated by V_T changes. It might be ascribed to the violation of assumptions: the arterial input time–activity curve has a consistent pattern from study to study, and the area under the curve of time–activity curve is proportional to the injected dose per body weight. Our study clearly indicated the violation of these assumptions in the case of TSPO imaging. Therefore, using only brain SUV to quantify TSPO binding has its limitations.

Effect of Blood Centrifugation

Switching to immediate centrifugation improved the test–retest reliability in blood significantly. Because TSPO is also expressed in blood, for example, in monocytes (*2*), we hypothesized that ^{123}I-CLINDE continues to bind to TSPO in blood cells and that intact ^{123}I-CLINDE in a blood sample will gradually bind to blood cells causing an underestimation of plasma radioactivity. Our hypothesis is supported by the increase in PoB ratio by immediate centrifugation. The negative correlation between PoB in MABs and monocyte counts also indicate that CLINDE binding is related to TSPO expression in blood. Additionally, the lower starting point of PoB time–activity curve of HABs than time–activity curve of MABs (Supplemental Fig. 1) indicates that binding of CLINDE to blood cells is dependent on the affinity/TSPO polymorphism (*21*). Previously, in Rizzo et al. (*22*) an extra compartment was proposed to describe TSPO ligand binding to the vascular walls. On the basis of our observations, the endothelial compartment may additionally include binding TSPO in blood cells.

However, fast and systematic centrifugation of blood samples will still be required to produce consistent results.

CONCLUSION

The variability of ^{123}I-CLINDE binding was investigated in a test–retest setting with 16 healthy subjects. The test–retest variability estimated by ICC and PD was favorable compared with the first-generation TSPO ligand ^{11}C-PK11195 and comparable to or slightly better than second-generation TSPO ligands ^{11}C-DPA-713 and ^{11}C-PBR28. SUV as a surrogate of the output measure V_T from gold standard 2TCM has its limitations. Immediate centrifugation of blood samples is essential and can prevent underestimation of the plasma input function. A population-based method could efficiently recover data with delayed centrifugation and has the potential to be applied to studies using other TSPO ligands.

DISCLOSURE

This work was financially supported by the European Union's Seventh Framework Program (FP7/2007-2013) under grant agreement no. HEALTH-F2-2011-278850 (INMiND) and the Danish Council for Independent Research (grant ID 0602-0228-8B). No other potential conflict of interest relevant to this article was reported.

ACKNOWLEDGMENTS

We acknowledge Svitlana Olsen and Glenna Skouboe for technical assistance and Brice Ozenne for his assistance in statistical analysis.

REFERENCES

1. Papadopoulos V, Baraldi M, Guilarte TR, et al. Translocator protein (18kDa): new nomenclature for the peripheral-type benzodiazepine receptor based on its structure and molecular function. *Trends Pharmacol Sci.* 2006;27:402–409.
2. Canat X, Carayon P, Bouaboula M, et al. Distribution profile and properties of peripheral-type benzodiazepine receptors on human hemopoietic cells. *Life Sci.* 1993;52:107–118.
3. Chen MK, Guilarte TR. Translocator protein 18 kDa (TSPO): molecular sensor of brain injury and repair. *Pharmacol Ther.* 2008;118:1–17.
4. Papadopoulos V, Lecanu L. Translocator protein (18 kDa) TSPO: an emerging therapeutic target in neurotrauma. *Exp Neurol.* 2009;219:53–57.
5. Takano A, Piehl F, Hillert J, et al. In vivo TSPO imaging in patients with multiple sclerosis: a brain PET study with [^{18}F]FEDAA1106. *EJNMMI Res.* 2013;3:30.
6. Winkeler A, Boisgard R, Awde AR, et al. The translocator protein ligand [^{18}F] DPA-714 images glioma and activated microglia in vivo. *Eur J Nucl Med Mol Imaging.* 2012;39:811–823.
7. Jučaite A, Cselenyi Z, Arvidsson A, et al. Kinetic analysis and test-retest variability of the radioligand [^{11}C](R)-PK11195 binding to TSPO in the human brain: a PET study in control subjects. *EJNMMI Res.* 2012;2:15.
8. Coughlin JM, Wang Y, Ma S, et al. Regional brain distribution of translocator protein using [^{11}C]DPA-713 PET in individuals infected with HIV. *J Neurovirol.* 2014;20:219–232.
9. Collste K, Forsberg A, Varrone A, et al. Test-retest reproducibility of [^{11}C] PBR28 binding to TSPO in healthy control subjects. *Eur J Nucl Med Mol Imaging.* 2016;43:173–183.
10. Park E, Gallezot JD, Delgadillo A, et al. ^{11}C-PBR28 imaging in multiple sclerosis patients and healthy controls: test-retest reproducibility and focal visualization of active white matter areas. *Eur J Nucl Med Mol Imaging.* 2015;42:1081–1092.
11. Arlicot N, Katsifis A, Garreau L, et al. Evaluation of CLINDE as potent translocator protein (18 kDa) SPECT radiotracer reflecting the degree of neuroinflammation in a rat model of microglial activation. *Eur J Nucl Med Mol Imaging.* 2008;35:2203–2211.
12. Feng L, Svarer C, Thomsen G, et al. In vivo quantification of cerebral translocator protein binding in humans using 6-chloro-2-(4′-^{123}I-iodophenyl)-3-(*N*,*N*-diethyl)-imidazo[1,2-a]pyridine-3-acetamide SPECT. *J Nucl Med.* 2014;55:1966–1972.
13. Jensen P, Feng L, Law I, et al. TSPO imaging in glioblastoma multiforme: a direct comparison between ^{123}I-CLINDE SPECT, ^{18}F-FET PET, and gadolinium-enhanced MR imaging. *J Nucl Med.* 2015;56:1386–1390.
14. Jensen P, Kondziella D, Thomsen G, Dyssegaard A, Svarer C, Pinborg LH. Anti-NMDAR encephalitis: demonstration of neuroinflammation and the effect of immunotherapy. *Neurology.* 2015;84:859.
15. Owen DR, Yeo AJ, Gunn RN, et al. An 18-kDa translocator protein (TSPO) polymorphism explains differences in binding affinity of the PET radioligand PBR28. *J Cereb Blood Flow Metab.* 2012;32:1–5.
16. Gillings N. A restricted access material for rapid analysis of [^{11}C]-labeled radiopharmaceuticals and their metabolites in plasma. *Nucl Med Biol.* 2009;36:961–965.
17. Willendrup P, Pinborg LH, Hasselbalch SG, et al. Assessment of the precision in co-registration of structural MR images and PET images with localized binding. *Int Congr Ser.* 2004;1265:275–280.
18. Svarer C, Madsen K, Hasselbalch SG, et al. MR-based automatic delineation of volumes of interest in human brain PET images using probability maps. *Neuroimage.* 2005;24:969–979.
19. Thie JA. Understanding the standardized uptake value, its methods, and implications for usage. *J Nucl Med.* 2004;45:1431–1434.
20. Yoder KK, Territo PR, Hutchins GD, et al. Comparison of standardized uptake values with volume of distribution for quantitation of [^{11}C]PBR28 brain uptake. *Nucl Med Biol.* 2015;42:305–308.
21. Kanegawa N, Collste K, Forsberg A, et al. In vivo evidence of a functional association between immune cells in blood and brain in healthy human subjects. *Brain Behav Immun.* 2016;54:149–157.
22. Rizzo G, Veronese M, Tonietto M, Zanotti-Fregonara P, Turkheimer FE, Bertoldo A. Kinetic modeling without accounting for the vascular component impairs the quantification of [^{11}C]PBR28 brain PET data. *J Cereb Blood Flow Metab.* 2014;34:1060–1069.